Double Higher Order Method of Moments for Surface Integral Equation Modeling of Metallic and Dielectric Antennas and Scatterers

Miroslav Djordjević, *Member, IEEE,* and Branislav M. Notaroš, *Senior Member, IEEE*

***Abstract*—A novel double higher order Galerkin-type method of moments based on higher order geometrical modeling and higher order current modeling is proposed for surface integral equation analysis of combined metallic and dielectric antennas and scatterers of arbitrary shapes. The technique employs generalized curvilinear quadrilaterals of arbitrary geometrical orders for the approximation of geometry (metallic and dielectric surfaces) and hierarchical divergence-conforming polynomial vector basis functions of arbitrary orders for the approximation of electric and magnetic surface currents within the elements. The geometrical orders and current-approximation orders of the elements are entirely independent from each other, and can be combined independently for the best overall performance of the method in different applications. The results obtained by the higher order technique are validated against the analytical solutions and the numerical results obtained by low-order moment-method techniques from literature. The examples show excellent accuracy, flexibility, and efficiency of the new technique at modeling of both current variation and curvature, and demonstrate advantages of large-domain models using curved quadrilaterals of high geometrical orders with basis functions of high current-approximation orders over commonly used small-domain models and low-order techniques. The reduction in the number of unknowns is by an order of magnitude when compared to low-order solutions.**

***Index Terms*—Electromagnetic analysis, electromagnetic scattering, higher order modeling, integral equations, method of moments (MoM).**

I. Introduction

ANTENNAS involved in modern wireless systems are often composed of metallic and dielectric parts of arbitrary shapes and with arbitrary curvature. There is a clear need for advanced analysis and design tools for predicting the performance and optimizing the parameters of such antennas prior to costly prototype development. These tools have to be based on general computational electromagnetic methods for modeling of arbitrary three-dimensional (3-D) combined metallic and dielectric structures. In addition, antenna designers demand that the simulation tools be accurate, fast, reliable, and run on relatively small computing platforms, such as standard desktop PCs.

One of the most general approaches to the analysis of metallic and dielectric structures is the surface integral equation (SIE) approach, where both electric and magnetic surface currents are introduced over boundary surfaces between homogeneous parts of the structure, and surface integral equations based on boundary conditions for both electric and magnetic field intensity vectors are solved with current densities as unknowns. The SIEs are discretized by the method of moments (MoM) [1], which gives rise to MoM-SIE modeling techniques [2]–[4]. Overall, the MoM-SIE method is an extremely powerful and versatile numerical methodology for electromagnetic-field simulation in antenna and scattering applications that involve perfectly conducting and penetrable (dielectric and linear magnetic) materials.

However, practically all the existing 3-D MoM-SIE simulation tools for metallic/dielectric structures are low-order or small-domain (subdomain) techniques—the structure is modeled by surface geometrical elements (boundary elements) that are electrically very small and the electric and magnetic currents over the elements are approximated by low-order (zeroth-order and first-order) basis functions. More precisely, the boundary elements (patches) are on the order of $\lambda/10$ in each dimension, λ being the wavelength in the medium. This results in a very large number of unknowns (unknown current-distribution coefficients) needed to obtain results of satisfactory accuracy, with all the associated problems and enormous requirements in computational resources. In addition, commonly used boundary elements are in the form of flat triangular and quadrilateral patches, and thus they do not provide enough flexibility and efficiency in modeling of structures with pronounced curvature.

An alternative which can greatly reduce the number of unknowns for a given problem and enhance further the accuracy and efficiency of the MoM-SIE analysis in antenna/scattering applications is the higher order or large-domain computational approach. According to this approach, a structure is approximated by a number of as large as possible geometrical elements, and the approximation of current components within individual elements is in the form of a single (two-fold) functional series of sufficiently high order. Only relatively recently the computational electromagnetics (CEM) community has started to extensively investigate and employ higher order surface and volume elements and higher order basis functions in the frame of MoM, including both the SIE formulation [5]–[9] and volume integral equation (VIE) formulation [10]–[15], and the finite element method (FEM) [6], [16]–[20].

For MoM-SIE modeling of general structures that may possess arbitrary curvature, it is essential to have both higher order geometrical flexibility for curvature modeling and higher order

Manuscript received February 14, 2003; revised August 4, 2003. This work was supported by the National Science Foundation under Grant ECS-0115756.

The authors are with the Department of Electrical and Computer Engineering, University of Massachusetts Dartmouth, Dartmouth, MA 02747-2300 USA (e-mail: miroslav@ieee.org; bnotaros@umassd.edu).

Digital Object Identifier 10.1109/TAP.2004.833175

current-approximation flexibility for current modeling in the same method. In other words, if higher order (large-domain) basis functions for currents are used on flat patches, many small patches may be required for the geometrical precision of the model, and then higher order basis functions actually reduce to low-order functions (on small patches). On the other hand, geometrical flexibility of curved patches can be fully exploited only if they can be made electrically large, which implies the use of higher order current expansions within the elements as well. Finally, in order to make the modeling of realistic structures optimal, it is convenient to have elements of different orders and sizes combined together in the same model. If all of these requirements are to be satisfied, implementation of hierarchical-type higher order polynomial basis functions for the approximation of electric and magnetic surface currents over curved boundary elements seems to be the right choice.

This paper proposes a novel higher order (large-domain) PC-oriented Galerkin-type MoM-SIE technique for 3-D electromagnetics based on higher order geometrical modeling and higher order current modeling, which we refer to as a double higher order method. The surface elements proposed for the approximation of geometry (metallic and dielectric surfaces) are generalized curvilinear quadrilaterals of arbitrary geometrical orders. The basis functions proposed for the approximation of currents within the elements are hierarchical divergence-conforming polynomial vector basis functions of arbitrary orders. The proposed technique represents a generalization of the MoM-SIE technique [9], where bilinear quadrilateral surface elements (boundary elements of the first geometrical order) are used with higher order polynomial current expansions. The new method enables excellent curvature modeling (e.g., a sphere is practically perfectly modeled by only six curved quadrilateral boundary elements of the fourth geometrical order) and excellent current-distribution modeling (e.g., using the eighth-order polynomial current-approximation in the two parametric coordinates on a quadrilateral boundary element). This enables using large curved MoM quadrilaterals that are on the order of λ (e.g., $1.5\lambda - 2\lambda$) in each dimension as building blocks for modeling of the electromagnetic structure (i.e., the boundary elements can be by two orders of magnitude larger in area than traditional low-order boundary elements). Element orders in the model, however, can also be low, so that the lower order modeling approach is actually included in the higher order modeling. The geometrical orders and current-approximation orders of the elements are entirely independent from each other, and the two sets of parameters of the double higher order model can be combined independently for the best overall performance of the method. Because the proposed basis functions are hierarchical, a whole spectrum of element sizes with the corresponding current-approximation orders can be used at the same time in a single simulation model of a complex structure. Additionally, each individual element can have drastically different edge lengths, enabling a whole range of "regular" and "irregular" element shapes (e.g., square-shaped, rectangular, strip-like, trapezoidal, triangle-like, etc.) to be used in a simulation model as well. Some preliminary results of double-higher order MoM modeling of purely metallic structures are presented in [21].

This paper is organized as follows. Section II presents the mathematical development of the proposed boundary elements and describes numerical components of the new double higher order MoM-SIE technique. This includes the derivation of surface integral equations for electric and magnetic surface current density vectors as unknown quantities, development of generalized Galerkin impedances (the system matrix elements) for arbitrary boundary elements (i.e., for any choice of surface elements for geometrical modeling and any choice of divergence-conforming basis functions for current modeling), generation of generalized curvilinear quadrilateral elements for higher order modeling of geometry, implementation of hierarchical polynomial vector basis functions for higher order modeling of currents over the quadrilaterals, and evaluation of generalized Galerkin impedances for the new proposed double higher order quadrilateral elements. In Section III, the accuracy, convergence, and efficiency of the new MoM-SIE technique are evaluated and discussed in several characteristic examples. The results obtained by the higher order MoM are compared with the analytical solutions and the numerical results obtained by low-order MoM techniques from literature. Numerical examples include a dihedral corner reflector, a metallic spherical scatterer (analyzed using six different higher order models), a dielectric spherical scatterer (analyzed using five different higher order models), and a circular cylinder of finite length with attached wire monopoles. The examples show excellent flexibility and efficiency of the new technique at modeling of both current variation and curvature, and demonstrate its advantages over low-order MoM techniques.

II. Novel Double Higher Order MoM for Electromagnetic Modeling

A. Surface Integral Equation Formulation

Consider an electromagnetic system consisting of arbitrarily shaped metallic and dielectric bodies. Let the system be excited by a time-harmonic electromagnetic field of complex field-intensities $\boldsymbol{E}_i$ and $\boldsymbol{H}_i$, and angular frequency ω. This field may be a combination of incident plane waves or the impressed field of one or more concentrated generators. According to the surface equivalence principle (generalized Huygens' principle), we can break the entire system into subsystems, each representing one of the dielectric regions (domains), together with the belonging metallic surfaces, with the remaining space being filled with the same medium. One of the domains is the external space surrounding the structure. The scattered electric and magnetic fields, $\boldsymbol{E}$ and $\boldsymbol{H}$, in each domain can be expressed in terms of the equivalent (artificial) surface electric current, of density $\boldsymbol{J}_S$, and equivalent (artificial) surface magnetic currents, of density $\boldsymbol{M}_S$, which are placed on the boundary surface of the domain, with the objective to produce a zero total field in the surrounding space. On the metallic surfaces, only the surface electric currents ($\boldsymbol{J}_S$) exist (these are actual currents) and $\boldsymbol{M}_S = 0$.

The boundary conditions for the tangential components of the total (incident plus scattered) electric and magnetic field vectors on the boundary surface between any two adjacent dielectric domains (domains 1 and 2) yield

$$[\boldsymbol{E}(\boldsymbol{J}_S,\boldsymbol{M}_S,\varepsilon_1,\mu_1)]_{\text{tang}}+(\boldsymbol{E}_i)_{\text{tang}} = [\boldsymbol{E}(-\boldsymbol{J}_S,-\boldsymbol{M}_S,\varepsilon_2,\mu_2)]_{\text{tang}} \quad (1)$$

$$[\boldsymbol{H}(\boldsymbol{J}_S,\boldsymbol{M}_S,\varepsilon_1,\mu_1)]_{\text{tang}}+(\boldsymbol{H}_i)_{\text{tang}} = [\boldsymbol{H}(-\boldsymbol{J}_S,-\boldsymbol{M}_S,\varepsilon_2,\mu_2)]_{\text{tang}} \quad (2)$$

where we assume that the incident (impressed) field is present only in domain 1. On the conducting bodies, the boundary conditions (1) and (2) reduce to $(\boldsymbol{E}_{\text{tot}})_{\text{tang}}=0$ only, so for metallic surfaces in domain 1 we have

$$[\boldsymbol{E}(\boldsymbol{J}_S,\boldsymbol{M}_S,\varepsilon_1,\mu_1)]_{\text{tang}}+(\boldsymbol{E}_i)_{\text{tang}}=0. \quad (3)$$

The scattered electric field in the region of complex permittivity ε and complex permeability μ is expressed in terms of the electric and magnetic current densities as follows:

$$\boldsymbol{E}=\boldsymbol{E}_J(\boldsymbol{J}_S)+\boldsymbol{E}_M(\boldsymbol{M}_S) \quad (4)$$

$$\boldsymbol{E}_J(\boldsymbol{J}_S)=-j\omega\boldsymbol{A}-\nabla\phi \quad (5)$$

$$\boldsymbol{E}_M(\boldsymbol{M}_S)=-\frac{1}{\varepsilon}\nabla\times\boldsymbol{F} \quad (6)$$

while the scattered magnetic field is obtained as

$$\boldsymbol{H}=\boldsymbol{H}_M(\boldsymbol{M}_S)+\boldsymbol{H}_J(\boldsymbol{J}_S) \quad (7)$$

$$\boldsymbol{H}_M(\boldsymbol{M}_S)=-j\omega\boldsymbol{F}-\nabla U \quad (8)$$

$$\boldsymbol{H}_J(\boldsymbol{J}_S)=\frac{1}{\mu}\nabla\times\boldsymbol{A}. \quad (9)$$

In the above expressions, $\boldsymbol{A}$ and $\boldsymbol{F}$ are the magnetic and electric vector potentials, and Φ and U are the electric and magnetic scalar potentials, respectively. The potentials are given by

$$\boldsymbol{A}=\mu\int_S \boldsymbol{J}_S g\,dS \quad (10)$$

$$\boldsymbol{F}=\varepsilon\int_S \boldsymbol{M}_S g\,dS \quad (11)$$

$$\Phi=\frac{j}{\omega\varepsilon}\int_S \nabla_S\cdot\boldsymbol{J}_S g\,dS \quad (12)$$

$$U=\frac{j}{\omega\mu}\int_S \nabla_S\cdot\boldsymbol{M}_S g\,dS \quad (13)$$

where S is the boundary surface of the considered domain, and g the Green's function for the unbounded homogeneous medium of parameters ε and μ

$$g=\frac{\mathrm{e}^{-\gamma R}}{4\pi R},\quad \gamma=j\omega\sqrt{\varepsilon\mu} \quad (14)$$

γ being the propagation coefficient in the medium and R the distance of the field point from the source point.

Having in mind the integral expressions for fields $\boldsymbol{E}$ and $\boldsymbol{H}$ in (4)–13, (1)–(3) represent a set of coupled electric/magnetic field integral equations (EFIE/MFIE) for $\boldsymbol{J}_S$ and $\boldsymbol{M}_S$ as unknowns, which can be discretized and solved using the MoM.

B. Generalized Galerkin Impedances for Arbitrary Surface Elements

Assume first that all the surfaces (metallic and dielectric) in the system are approximated by a number of arbitrary surface elements. Let us approximate the surface electric and magnetic current density vectors, $\boldsymbol{J}_S$ and $\boldsymbol{M}_S$, over every element in the model by a convenient set of basis functions with unknown complex current-distribution coefficients. In order to determine these coefficients, the EFIE/MFIE system in (1)–(3) is tested by means of the Galerkin method, i.e., using the same functions used for current expansion. The four types of generalized Galerkin impedances (the system matrix elements) corresponding to the four combinations of electric- and magnetic-current testing functions $\boldsymbol{J}_{Sm}$ and $\boldsymbol{M}_{Sm}$ defined on the mth surface element (S_m) and the electric- and magnetic-current basis functions $\boldsymbol{J}_{Sn}$ and $\boldsymbol{M}_{Sn}$ defined on the nth element in the model are given by

$$Z_{\text{mn}}^{\text{ee}}=\int_{S_m}\boldsymbol{J}_{Sm}\cdot\boldsymbol{E}_J(\boldsymbol{J}_{Sn})dS_m \quad (15)$$

$$Z_{\text{mn}}^{\text{em}}=\int_{S_m}\boldsymbol{J}_{Sm}\cdot\boldsymbol{E}_M(\boldsymbol{M}_{Sn})dS_m \quad (16)$$

$$Z_{\text{mn}}^{\text{me}}=\int_{S_m}\boldsymbol{M}_{Sm}\cdot\boldsymbol{H}_J(\boldsymbol{J}_{Sn})dS_m \quad (17)$$

$$Z_{\text{mn}}^{\text{mm}}=\int_{S_m}\boldsymbol{M}_{Sm}\cdot\boldsymbol{H}_M(\boldsymbol{M}_{Sn})dS_m. \quad (18)$$

The generalized voltages (the excitation column-matrix elements) are evaluated as

$$V_m^{\text{e}}=-\int_{S_m}\boldsymbol{J}_{Sm}\cdot\boldsymbol{E}_i dS_m \quad (19)$$

$$V_m^{\text{m}}=-\int_{S_m}\boldsymbol{M}_{Sm}\cdot\boldsymbol{H}_i dS_m. \quad (20)$$

Substituting (5) into (15), expanding $\nabla_S\cdot(\boldsymbol{J}_{Sm}\phi_n)$, and applying the surface divergence theorem leads to the following expressions for electric/electric Galerkin impedances:

$$\begin{aligned}Z_{\text{mn}}^{\text{ee}}&=-j\omega\int_{S_m}\boldsymbol{J}_{Sm}\cdot\boldsymbol{A}_n dS_m-\int_{S_m}\boldsymbol{J}_{Sm}\cdot\nabla_S\phi_n dS_m\\&=-j\omega\int_{S_m}\boldsymbol{J}_{Sm}\cdot\boldsymbol{A}_n dS_m+\int_{S_m}\phi_n\nabla_S\cdot\boldsymbol{J}_{Sm}dS_m\\&\quad-\oint_{c_m}\boldsymbol{J}_{Sm}\phi_n\boldsymbol{n}_m dl_m\end{aligned} \quad (21)$$

where $\boldsymbol{n}_m$ is the outward normal to the boundary contour C_m of the surface S_m. When the divergence-conforming current expansion on boundary elements is used, the last term in (21) is identically equal to zero, because the normal components of testing functions $\boldsymbol{J}_{Sm}$ are either zero at the element edges or the two contributions of the elements sharing an edge exactly cancel out in the final expressions for generalized impedances. Finally,

expressing the potentials in (21) in terms of the electric-current basis function $\boldsymbol{J}_{Sn}$ over the nth surface element (S_n), we obtain

$$Z_{\mathrm{mn}}^{\mathrm{ee}} = -j\omega\mu \int_{S_m}\int_{S_n} \boldsymbol{J}_{Sm}\cdot\boldsymbol{J}_{Sn} g dS_n dS_m + \frac{j}{\omega\varepsilon}\int_{S_m}\int_{S_n} (\nabla_S\cdot\boldsymbol{J}_{Sm})(\nabla_S\cdot\boldsymbol{J}_{Sn}) g dS_n dS_m. \quad (22)$$

Similarly, starting with (6) and (11), expanding $\nabla\times(\boldsymbol{M}_n g)$, and performing a cyclic permutation of the scalar triple product, the expression for electric/magnetic generalized impedances in (16) can be transformed to read

$$\begin{aligned} Z_{\mathrm{mn}}^{\mathrm{em}} &= -\frac{1}{\varepsilon}\int_{S_m}\boldsymbol{J}_{Sm}\cdot\nabla\times\boldsymbol{F}_n dS_m \\ &= -\int_{S_m}\int_{S_n}\boldsymbol{J}_{Sm}\cdot\nabla\times(\boldsymbol{M}_{Sn}g) dS_n dS_m \\ &= -\int_{S_m}\int_{S_n}\boldsymbol{J}_{Sm}\cdot(\nabla g\times\boldsymbol{M}_{Sn}) dS_n dS_m \\ &= -\int_{S_m}\int_{S_n}(\boldsymbol{M}_{Sn}\times\boldsymbol{J}_{Sm})\cdot\nabla g dS_n dS_m. \end{aligned} \quad (23)$$

By duality, the magnetic/electric and magnetic/magnetic generalized Galerkin impedances in (17) and (18) have the same respective forms as those in (23) and (22), and are given by

$$\begin{aligned} Z_{\mathrm{mn}}^{\mathrm{me}} &= -\int_{S_m}\int_{S_n}(\boldsymbol{J}_{Sn}\times\boldsymbol{M}_{Sm})\cdot\nabla g dS_n dS_m \\ &= -Z_{\mathrm{mn}}^{\mathrm{em}}, \end{aligned} \quad (24)$$

$$Z_{\mathrm{mn}}^{\mathrm{mm}} = -j\omega\varepsilon\int_{S_m}\int_{S_n}\boldsymbol{M}_{Sm}\cdot\boldsymbol{M}_{Sn} g dS_n dS_m + \frac{j}{\omega\mu}\int_{S_m}\int_{S_n}(\nabla_S\cdot\boldsymbol{M}_{Sm})(\nabla_S\cdot\boldsymbol{M}_{Sn}) g dS_n dS_m. \quad (25)$$

Equations (22)–(25) provide general expressions for MoM generalized impedances for solving the EFIE/MFIE in (1)–(3) using any type of surface discretization and any adopted set of divergence-conforming basis functions in the context of the Galerkin method. In what follows, we shall restrict our attention to the specific higher order MoM technique proposed for analysis of electromagnetic radiation and scattering in this paper.

C. Higher Order Geometrical Modeling

As basic building blocks for geometrical modeling of 3-D electromagnetic structures of arbitrary shape and material composition, we propose generalized curved parametric quadrilaterals of higher (theoretically arbitrary) geometrical orders (Fig. 1). A generalized quadrilateral is determined by $M=(K_u+1)(K_v+1)$ points (interpolation nodes) arbitrarily positioned in space, where K_u and K_v (K_u, $K_v \geq 1$) are geometrical orders of the element along u- and v- parametric coordinates, respectively (note that the orders do not need to be the same within an element). The quadrilateral can be described analytically as

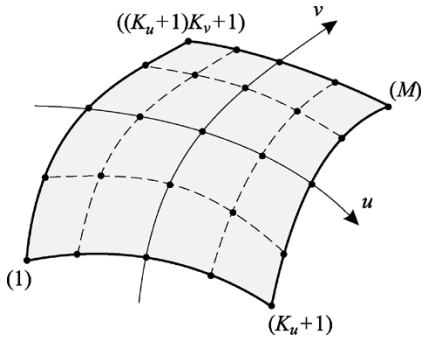

Fig. 1. Generalized parametric quadrilateral of geometrical orders K_u and $K_v (K_u, K_v \geq 1)$. $M = (K_u+1)(K_v+1)$ is the total number of interpolation points.

$$\boldsymbol{r}(u,v)=\sum_{i=1}^{M}\boldsymbol{r}_i p_i(u,v)=\sum_{k=0}^{K_u}\sum_{l=0}^{K_v}\boldsymbol{r}_{kl}u^k v^l, \quad -1\leq u,v\leq 1 \quad (26)$$

where $\boldsymbol{r}_1,\boldsymbol{r}_2,\ldots,\boldsymbol{r}_M$ are the position vectors of the interpolation nodes, $p_i(u,v)$ are Lagrange-type interpolation polynomials satisfying the Kronecker delta relation $p_i(u_j,v_j)=\delta_{ij}$, with u_j and v_j representing the parametric coordinates of the jth node, and $\boldsymbol{r}_{kl}$ are constant vector coefficients related to $\boldsymbol{r}_1,\boldsymbol{r}_2,\ldots,\boldsymbol{r}_M$. For more details on geometrical properties of parametric elements (in the context of FEM) the reader is referred to [22], [23].

In this paper, we use the equidistant distribution of interpolation nodes along each coordinate in the parametric space, while the use of specific nonequidistant node distributions, which would provide additional modeling flexibility and accuracy in some applications, is possible as well. In addition, any other choice of higher order surface expansions for geometrical modeling that can be represented as a double sum of 2-D power functions $u^k v^l$ (e.g., parametric quadrilaterals using spline functions for describing the geometry) can also readily be implemented in our method for electromagnetic analysis.

Note that, in general, the surface tangent is discontinuous on the boundary of two attached curved generalized parametric quadrilateral elements defined by (26), regardless of the geometrical orders K_u and K_v of the quadrilaterals. However, this geometrical discontinuity across the boundaries of adjacent elements becomes less pronounced as the elements of higher geometrical orders are used. For instance, when approximating a circular cylinder using 32 interpolation points along its circumference and three different geometrical models constructed from: (A) 32 first-order $(K_u=K_v=1)$ elements; (B) 16 second-order $(K_u=K_v=2)$ elements; and (C) eight fourth-order $(K_u=K_v=4)$ elements per cylinder circumference, the angles between the surface tangents of the neighboring elements at the junctions in models (A), (B), and (C) are 168.750°, 179.787°, and 180.011°, respectively, compared to the exact 180°. If a more accurate model is needed, one can increase the total number and/or geometrical orders of patches. Note also that this geometrical problem is not present if the geometry is

described in terms of spline functions, which can provide continuous surface tangents across the edges shared by curved elements (e.g., third-order splines used to solve scattering from bodies of revolution in [24]).

All the geometries considered as examples in this paper are modeled using specialized geometrical preprocessor codes, and no general meshers are employed. Development and discussions of general geometrical preprocessors for mesh generation for an arbitrary geometry using higher order surface elements is beyond the scope of this paper.

D. Higher Order Basis Functions for Electric and Magnetic Currents

Electric and magnetic surface current density vectors over every generalized quadrilateral in the model are represented as

$$\begin{aligned}\boldsymbol{J}_S(u,v) &= \sum_{i=0}^{N_u}\sum_{j=0}^{N_v-1}\alpha_{uij}\boldsymbol{f}_{uij}(u,v) \\ &\quad + \sum_{i=0}^{N_u-1}\sum_{j=0}^{N_v}\alpha_{vij}\boldsymbol{f}_{vij}(u,v) \qquad (27)\\ \boldsymbol{M}_S(u,v) &= \sum_{i=0}^{N_u}\sum_{j=0}^{N_v-1}\beta_{uij}\boldsymbol{f}_{uij}(u,v) \\ &\quad + \sum_{i=0}^{N_u-1}\sum_{j=0}^{N_v}\beta_{vij}\boldsymbol{f}_{vij}(u,v) \qquad (28)\end{aligned}$$

where $\boldsymbol{f}$ are divergence-conforming hierarchical-type vector basis functions defined as

$$\begin{aligned}\boldsymbol{f}_{uij}(u,v) &= \frac{P_i(u)v^j}{J(u,v)}\boldsymbol{a}_u(u,v)\\ \boldsymbol{f}_{vij}(u,v) &= \frac{u^iP_j(v)}{J(u,v)}\boldsymbol{a}_v(u,v)\\ P_i(u) &= \begin{cases}1-u, & i=0\\ u+1, & i=1\\ u^i-1, & i\geq 2, \text{ even}\\ u^i-u, & i\geq 3, \text{ odd}\end{cases}\\ &\quad -1\leq u,v\leq 1. \qquad (29)\end{aligned}$$

Parameters N_u and N_v are the adopted degrees of the polynomial current approximation, which are entirely independent from the element geometrical orders (K_u and K_v), and α_{uij}, α_{vij}, β_{uij}, and β_{vij} are unknown current-distribution coefficients. The unitary vectors $\boldsymbol{a}_u$ and $\boldsymbol{a}_v$ in (29) are obtained as

$$\boldsymbol{a}_u(u,v) = \frac{\partial \boldsymbol{r}(u,v)}{\partial u}, \quad \boldsymbol{a}_v(u,v) = \frac{\partial \boldsymbol{r}(u,v)}{\partial v} \qquad (30)$$

with $\boldsymbol{r}$ given in (26), and J is the Jacobian of the covariant transformation

$$J(u,v) = \left|\boldsymbol{a}_u(u,v)\times\boldsymbol{a}_v(u,v)\right|. \qquad (31)$$

Note, that the sum limits in (27) and (28) that correspond to the variations of a current density vector component in the direction across that component are by one smaller than the orders corresponding to the variations in the other parametric coordinate. This mixed-order arrangement, which ensures equal approximation orders for surface charge densities corresponding to the u- and v-directed current basis functions, has been found to be a preferable choice for modeling of surface currents in all applications. It enables considerable reductions in the overall number of unknowns, at no expense in terms of the accuracy of current and charge modeling over surfaces. An excellent theoretical elaboration of this approach (in the context of FEM) can be found in [25].

E. Generalized Galerkin Impedances for Higher Order Quadrilateral Elements

The unknown coefficients $\{\alpha\}$ and $\{\beta\}$ in (27) and (28) are determined by solving the EFIE/MFIE system with the generalized Galerkin impedances given in (22)–(25), which we now specialize for the implementation of generalized curved quadrilateral elements of arbitrary geometrical orders, (26), and hierarchical divergence-conforming polynomial vector basis functions of arbitrary current-approximation orders, (29). Without the loss of generality, we consider only the u-components of basis and testing functions. Furthermore, we consider the functions in the following simplified form:

$$\boldsymbol{f}_{ij}(u,v) = \frac{\Gamma_{ij}(u,v)}{J(u,v)}\frac{\partial \boldsymbol{r}(u,v)}{\partial u} \qquad (32)$$

where Γ are the simple 2-D power functions

$$\Gamma_{ij}(u,v) = u^iv^j. \qquad (33)$$

The generalized Galerkin impedances corresponding to the complete basis functions in (29) can be obtained as a linear combination of those corresponding to the simplified functions in (32) and (33). In addition, the impedances for any higher order set of basis functions of divergence-conforming polynomial type can also be constructed as a linear combination of the impedances for the simple power functions in (32) and (33). A notable example may be higher order hierarchical basis functions with improved orthogonality properties constructed from ultraspherical and Chebyshev polynomials [26], [27] (note that the technique presented in [26], [27] is restricted to bilinear quadrilaterals (elements with $K_u = K_v = 1$) only, as well as that these basis functions, being more complicated than the regular polynomials, require larger MoM matrix filling times, and are therefore impractical when iterative solvers are not used).

Upon substituting (32) into (22), the electric/electric impedances corresponding to the testing function defined by indexes i_m and j_m on the mth quadrilateral and the basis function defined by indexes i_n and j_n on the nth quadrilateral become

$$\begin{aligned}Z^{\text{ee}}(i_m,j_m,i_n,j_n) &= -j\omega\mu\int_{u_{1m}}^{u_{2m}}\int_{v_{1m}}^{v_{2m}}\int_{u_{1n}}^{u_{2n}}\int_{v_{1n}}^{v_{2n}}\left(\Gamma_{i_mj_m}\frac{\partial \boldsymbol{r}_m}{\partial u_m}\right)\\ &\quad\cdot\left(\Gamma_{i_nj_n}\frac{\partial \boldsymbol{r}_n}{\partial u_n}\right)g(R)du_ndv_ndu_mdv_m\\ &\quad+\frac{j}{\omega\varepsilon}\int_{u_{1m}}^{u_{2m}}\int_{v_{1m}}^{v_{2m}}\int_{u_{1n}}^{u_{2n}}\int_{v_{1n}}^{v_{2n}}\frac{\partial\Gamma_{i_mj_m}}{\partial u_m}\frac{\partial\Gamma_{i_nj_n}}{\partial u_n}\\ &\quad\times g(R)du_ndv_ndu_mdv_m\\ &\quad i_m=0,1,\ldots,N_u^{(m)}\\ &\quad j_m=0,1,\ldots,N_v^{(m)}\\ &\quad i_n=0,1,\ldots,N_u^{(n)}\\ &\quad j_n=0,1,\ldots,N_v^{(n)} \qquad (34)\end{aligned}$$

where $N_u^{(m)}$ and $N_v^{(m)}$ are the current-approximation orders of the mth quadrilateral along the u- and v-coordinate, respectively, $N_u^{(n)}$ and $N_v^{(n)}$ are the corresponding orders for the nth quadrilateral, and the integration limits in both quadrilaterals are $u_1 = v_1 = -1$ and $u_2 = v_2 = 1$. The source-to-field distance R is computed as

$$R = \left|\boldsymbol{r}_m(u_m, v_m) - \boldsymbol{r}_n(u_n, v_n)\right|. \tag{35}$$

Taking into account the parametric representation of the quadrilateral surface element, (26), then leads to the final expression:

$$\begin{aligned} Z^{\mathrm{ee}}(i_m, j_m, i_n, j_n) = &\sum_{k_m=1}^{K_u^{(m)}} \sum_{l_m=0}^{K_v^{(m)}} \sum_{k_n=1}^{K_u^{(n)}} \sum_{l_n=0}^{K_v^{(n)}} k_m k_n \boldsymbol{r}_{kl}^{(m)} \cdot \boldsymbol{r}_{kl}^{(n)} \\ &\times \xi(i_m + k_m - 1, j_m + l_m, i_n + k_n - 1, \\ &\quad j_n + l_n) - \frac{1}{\omega^2 \mu \varepsilon} i_m i_n \\ &\times \xi(i_m - 1, j_m, i_n - 1, j_n) \end{aligned} \tag{36}$$

where $K_u^{(m)}$ and $K_v^{(m)}$ are the geometrical orders along the u- and v-coordinate, respectively, and $\boldsymbol{r}_{kl}^{(m)}$ are the geometrical vector coefficients in the polynomial expansion of the mth quadrilateral, $K_u^{(n)}$, $K_v^{(n)}$, and $\boldsymbol{r}_{kl}^{(n)}$ are the corresponding parameters for the nth quadrilateral in the model, and ξ is the basic Galerkin potential integral given by

$$\begin{aligned} \xi(i_m, j_m, i_n, j_n) = -j\omega\mu &\int_{u_{1m}}^{u_{2m}} \int_{v_{1m}}^{v_{2m}} \int_{u_{1n}}^{u_{2n}} \int_{v_{1n}}^{v_{2n}} u_m^{i_m} v_m^{j_m} u_n^{i_n} v_n^{j_n} \\ &\times g(R) du_n dv_n du_m dv_m. \end{aligned} \tag{37}$$

Similarly, using (32) and expanding the gradient of Green's function, the electric/magnetic impedances in (23) are transformed to

$$\begin{aligned} &Z^{\mathrm{em}}(i_m, j_m, i_n, j_n) \\ &\quad = -\frac{1}{\varepsilon} \int_{S_m} \boldsymbol{f}_m \nabla \times \boldsymbol{F}_n dS_m \\ &\quad = -\int_{u_{1m}}^{u_{2m}} \int_{v_{1m}}^{v_{2m}} \int_{u_{1n}}^{u_{2n}} \int_{v_{1n}}^{v_{2n}} \Gamma_{i_m j_m} \Gamma_{i_n j_n} \left(\frac{\partial \boldsymbol{r}_n}{\partial u_n} \times \frac{\partial \boldsymbol{r}_m}{\partial u_m} \right) \\ &\qquad \cdot \nabla g(R) du_n dv_n du_m dv_m \\ &\quad = -\int_{u_{1m}}^{u_{2m}} \int_{v_{1m}}^{v_{2m}} \int_{u_{1n}}^{u_{2n}} \int_{v_{1n}}^{v_{2n}} \Gamma_{i_m j_m} \Gamma_{i_n j_n} \left(\frac{\partial \boldsymbol{r}_n}{\partial u_n} \times \frac{\partial \boldsymbol{r}_m}{\partial u_m} \right) \\ &\qquad \cdot (\boldsymbol{r}_m - \boldsymbol{r}_n) \frac{1}{R} \frac{dg(R)}{dR} du_n dv_n du_m dv_m \\ &\qquad i_m = 0, 1, \ldots, N_u^{(m)}, \quad j_m = 0, 1, \ldots, N_v^{(m)} \\ &\qquad i_n = 0, 1, \ldots, N_u^{(n)}, \quad j_n = 0, 1, \ldots, N_v^{(n)}. \end{aligned} \tag{38}$$

Using (26) then yields

$$\begin{aligned} &Z^{\mathrm{em}}(i_m, j_m, i_n, j_n) \\ &\quad = \sum_{k'_m=0}^{K_u^{(m)}} \sum_{l'_m=0}^{K_v^{(m)}} \sum_{k_m=1}^{K_u^{(m)}} \sum_{l_m=0}^{K_v^{(m)}} \sum_{k_n=1}^{K_u^{(n)}} \sum_{l_n=0}^{K_v^{(n)}} k_m k_n \left(\boldsymbol{r}_{kl}^{(n)} \times \boldsymbol{r}_{kl}^{(m)} \right) \\ &\qquad \cdot \boldsymbol{r}_{k'l'}^{(m)} \zeta(i_m + k_m + k'_m - 1, j_m + l_m + l'_m, \\ &\qquad\quad i_n + k_n - 1, j_n + l_n) \\ &\quad - \sum_{k'_n=0}^{K_u^{(n)}} \sum_{l'_n=0}^{K_v^{(n)}} \sum_{k_m=1}^{K_u^{(m)}} \sum_{l_m=0}^{K_v^{(m)}} \sum_{k_n=1}^{K_u^{(n)}} \sum_{l_n=0}^{K_v^{(n)}} k_m k_n \left(\boldsymbol{r}_{kl}^{(n)} \times \boldsymbol{r}_{kl}^{(m)} \right) \\ &\qquad \cdot \boldsymbol{r}_{k'l'}^{(n)} \zeta(i_m + k_m - 1, j_m + l_m, \\ &\qquad\quad i_n + k_n + k'_n - 1, j_n + l_n + l'_n) \end{aligned} \tag{39}$$

where ζ is the basic Galerkin field integral evaluated as

$$\begin{aligned} \zeta(i_m, j_m, i_n, j_n) = -&\int_{u_{1m}}^{u_{2m}} \int_{v_{1m}}^{v_{2m}} \int_{u_{1n}}^{u_{2n}} \int_{v_{1n}}^{v_{2n}} u_m^{i_m} v_m^{j_m} u_n^{i_n} v_n^{j_n} \frac{1}{R} \\ &\times \frac{dg(R)}{dR} du_n dv_n du_m dv_m. \end{aligned} \tag{40}$$

Note that only two types of scalar basic Galerkin integrals, ξ and ζ in (37) and (40), are needed for the entire Galerkin impedance matrix. Moreover, only ξ-integrals are sufficient for purely metallic structures. These integrals are evaluated only once for any pair, m and n, of quadrilateral elements in the model. Rapid and accurate combined numerical/analytical methods are developed for the integration over curved higher order generalized quadrilateral surfaces, for the ξ- and ζ-integrals. When the distance R in (35) is relatively small (or zero), the procedure of extracting the (quasi)singularity is performed [28]. As can be expected, the problems with the (quasi)singular integration are more pronounced with the field integrals. Efficient algorithms for recursive construction of the generalized Galerkin impedances and the EFIE/MFIE system matrix are used in order to avoid redundant operations related to the summation indexes in the Gauss–Legendre integration formulas, as well as the indexes i and j for current expansions and k and l for geometrical representations within the impedances.

Starting with the generalized voltages given in (19) and (20), several models of lumped and distributed excitations and loads [29] are included in the proposed MoM technique (loads are introduced using the concept of a compensating electric field). The resulting system of linear algebraic equations with complex unknowns $\{\alpha\}$ and $\{\beta\}$ is solved classically, by the Gaussian elimination. By postprocessing of these coefficients, the currents $\boldsymbol{J}_S$ and $\boldsymbol{M}_S$ over any generalized quadrilateral in the model and fields $\boldsymbol{E}$ and $\boldsymbol{H}$ in any dielectric region (including the far field) are obtained.

III. Numerical Results and Discussion

A. Dihedral Corner Reflector

As an example of structures with flat surfaces, consider the scattering from a metallic 90° dihedral corner reflector. The two plates, each being $5.6088\lambda \times 5.6088\lambda$ large, are modeled by a total of $N_{\mathrm{el}} = 18$ bilinear quadrilateral elements ($K_u = K_v = 1$), which in this case reduce to squares, with the polynomial degrees $N_u = N_v = 8$ in all of the elements. Without the use of symmetry, this results in $N_{\mathrm{unkn}} = 2232$ unknowns. Fig. 2 shows the radar cross-section (RCS) of the reflector in the full azimuthal (horizontal) plane for the vertical polarization of the incident plane wave. The results obtained by the higher order

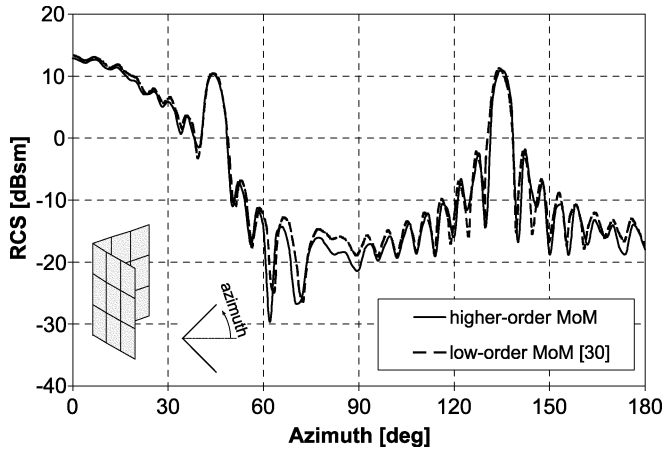

Fig. 2. Radar cross-section of a 90° dihedral corner reflector, in the full horizontal plane, for the vertical polarization of the incident plane wave, obtained by the higher order MoM and by the low-order MoM from [30].

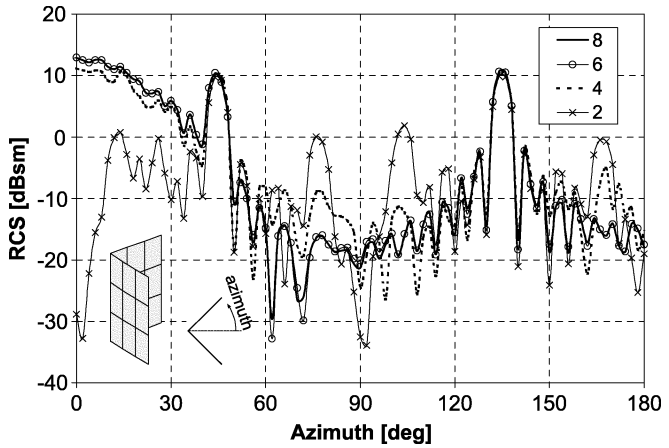

Fig. 3. Radar cross-section of a dihedral corner reflector for four different orders (2, 4, 6, and 8) of the polynomial approximation of currents in the higher order MoM.

MoM are compared with the low-order MoM results from [30] (the number of unknowns is not specified in [30]), and an excellent agreement is observed. Note that the quadrilaterals in the higher order model are 1.87λ on a side.

The convergence analysis of the higher order current approximation is performed for this example. Four different levels of the polynomial approximation of currents are adopted: (1) $N_u = N_v = 2$ ($N_{\text{unkn}} = 126$); (2) $N_u = N_v = 4$ ($N_{\text{unkn}} = 540$); (3) $N_u = N_v = 6$ ($N_{\text{unkn}} = 1242$); and (4) $N_u = N_v = 8$ ($N_{\text{unkn}} = 2232$). The corresponding RCS results are shown in Fig. 3. We observe excellent convergence properties of the polynomial basis functions, the RCS prediction average absolute differences between levels (1) and (2), (2) and (3), and (3) and (4), being 7.6, 3.4, and 0.3 dB, respectively. In specific, note that even the second-order current approximation yields accurate result for the lobes at the directions perpendicular to the dihedral sides. Additionally, with the fourth-order basis functions, the dominant double-reflected fields in the forward region of the reflector are also predicted reasonably accurately. Finally, the sixth-order (or higher) current-approximation model adds the accuracy in the computation of fields in the back region of the reflector as well. Note also that the estimated number

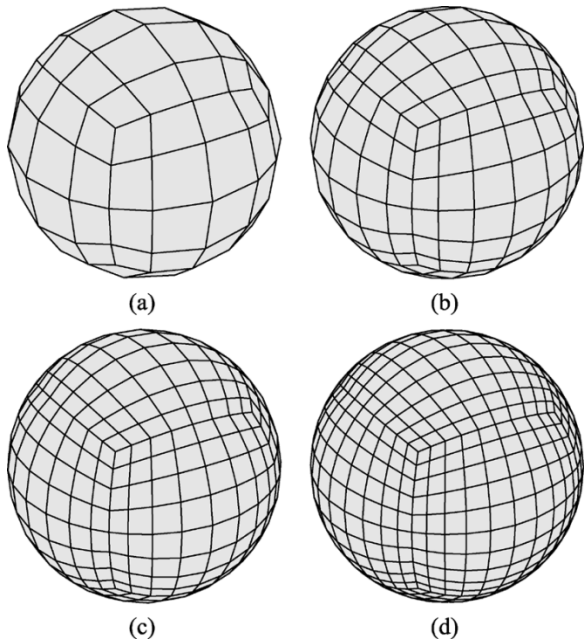

Fig. 4. Four geometrical models of a spherical scatterer constructed from (a) 96, (b) 216, (c) 384, and (d) 600 bilinear quadrilaterals ($K_u = K_v = 1$).

of unknowns, based on a topological analysis, for a common low-order MoM solution with the reflector subdivided into triangular patches with Rao–Wilton–Glisson (RWG) basis functions [31] is around 12000, which is about 10 times the number of unknowns required by the higher order MoM and $N_u = N_v = 6$.

B. Metallic Spherical Scatterer

As an example of curved metallic structures, consider a spherical metallic scatterer of radius $a = 1$ m illuminated by an incident plane electromagnetic wave in the frequency range 10–600 MHz. In the first set of experiments, the first-order geometrical modeling is employed ($K_u = K_v = 1$ in all elements). Four different geometrical models constructed from (1) $N_{\text{el}} = 6 \times (4 \times 4) = 96$ bilinear quadrilaterals [Fig. 4(a)], (2) $N_{\text{el}} = 6 \times (6 \times 6) = 216$ bilinear quadrilaterals [Fig. 4(b)], (3) $N_{\text{el}} = 6 \times (8 \times 8) = 384$ bilinear quadrilaterals [Fig. 4(c)], and (4) $N_{\text{el}} = 6 \times (10 \times 10) = 600$ bilinear quadrilaterals [Fig. 4(d)] are implemented, with the second-order current approximation ($N_u = N_v = 2$) in every element in all of the four models. The total numbers of unknowns without the use of symmetry in models (1), (2), (3), and (4) amount to $N_{\text{unkn}} = 768$, 1728, 3072, and 4800, respectively.

Shown in Fig. 5 is the RCS of the sphere, normalized to the sphere cross-section area, as a function of a/λ. The results obtained by the higher order MoM are compared with the analytical solution in the form of Mie's series. An excellent agreement between the numerical results obtained with the model (4) and analytical results is observed with the average absolute RCS prediction error less than 3%, while models (1), (2), and (3) provide acceptable results only up to the frequency at which $a/\lambda = 0.53$, 1, and 1.6, respectively [the results obtained by the model (1) are not shown in Fig. 5]. Note that an increase in the current-approximation orders N_u and N_v in models (1)–(3) does not yield better results at higher frequencies, meaning that the

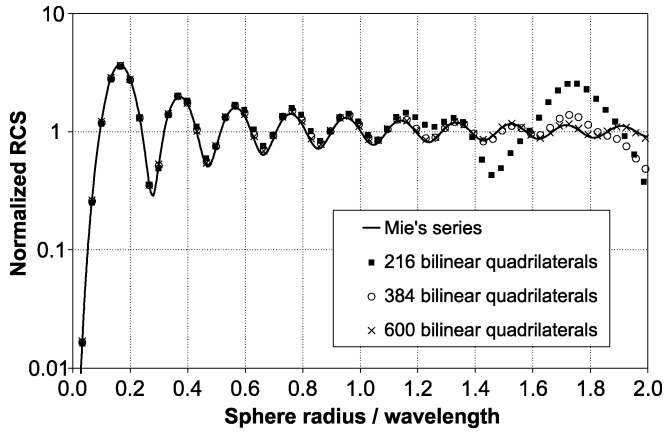

Fig. 5. Normalized radar cross-section $[\mathrm{RCS}/(a^2\pi)]$ of a metallic sphere, for three higher order MoM models employing the first-order geometrical modeling in Fig. 4(b)–(d), respectively, along with the exact solution (Mie's series).

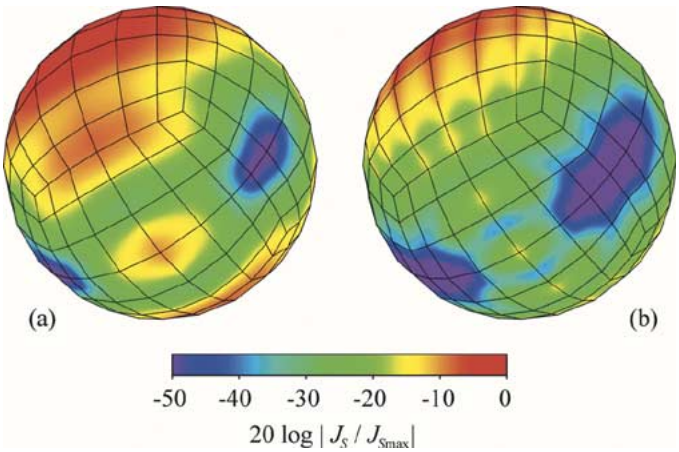

Fig. 6. Induced electric surface current over the surface of the model in Fig. 4(b) at two frequencies, corresponding to (a) $a/\lambda = 0.6$ and (b) $a/\lambda = 1.2$.

errors in the RCS prediction using these models are a consequence of the inaccuracy in geometrical modeling of the sphere surface. Note also that, even though this is an almost small-domain application of the proposed large-domain method, where a large number (600) of elements (with relatively low current approximation orders) is needed for the sphere surface to be geometrically accurately represented by parametric surfaces of the first geometrical order, the largest quadrilateral elements in the model (4) are 0.39λ on a side at the highest frequency considered, which is still considerably above the usual small-domain limit of 0.1λ.

For an additional insight into the correlation of errors in modeling of geometry and errors in modeling of currents, Fig. 6 shows the induced electric surface current over the surface of the model (2) at two frequencies, corresponding to (a) $a/\lambda = 0.6$ and (b) $a/\lambda = 1.2$. We observe that, while the mutual orientation of quadrilateral elements in the model at the frequency (a) does not influence the surface current distribution over the sphere surface, the interconnections and surface-tangent discontinuities between quadrilaterals at the frequency (b) act like wedges, and a nonphysical current distribution is

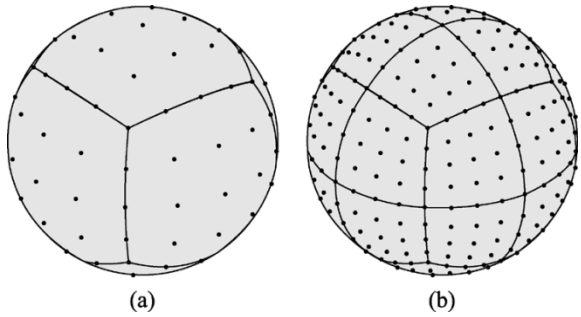

Fig. 7. Two geometrical models of a spherical scatterer constructed from (a) six and (b) 24 generalized quadrilaterals of the fourth geometrical order ($K_u = K_v = 4$).

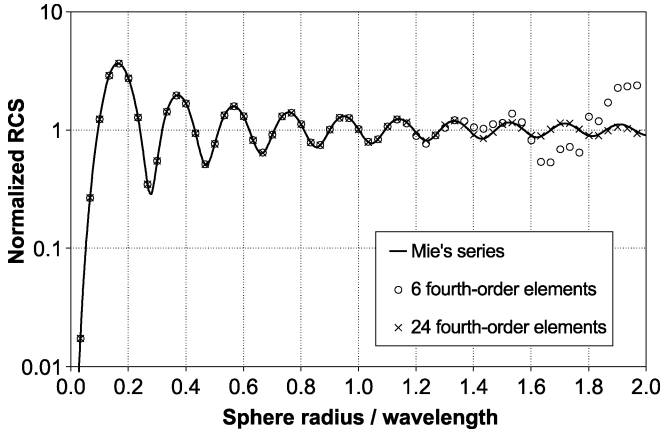

Fig. 8. Normalized radar cross-section $[\mathrm{RCS}/(a^2\pi)]$ of a metallic sphere, for two higher order MoM models employing the fourth-order geometrical modeling in Fig. 7(a) and (b), respectively, along with the exact solution (Mie's series).

obtained that follows the geometry of the quadrilateral mesh, where the variations of the current density magnitude clearly indicate the boundaries of the quadrilaterals constituting the model. These variations, of course, do not exist on the surface of the actual spherical scatterer. In other words, the error in modeling of curvature expressed in terms of the wavelength is negligible at the frequency (a), while at the frequency (b), it can not be ignored. The same conclusion is then translated from the current distribution consideration to the far field and RCS computation at frequencies (a) and (b), as can be observed from Fig. 5.

In the second set of experiments, the fourth-order geometrical modeling is employed ($K_u = K_v = 4$ in all elements). The sphere surface is first approximated by (A) $N_{\mathrm{el}} = 6$ fourth-order quadrilaterals [Fig. 7(a)] in conjunction with the eighth-order current approximation ($N_u = N_v = 8$) in each element and then by (B) $N_{\mathrm{el}} = 6 \times (2 \times 2) = 24$ fourth-order quadrilaterals [Fig. 7(b)] with the sixth-order current approximation ($N_u = N_v = 6$) in each element. This results in a total of $N_{\mathrm{unkn}} = 768$ and 1728 unknowns in models (A) and (B), respectively, with no symmetry used.

Fig. 8 shows the simulated RCS of the sphere obtained by the two geometrically higher order MoM models, as compared with the exact solution calculated in terms of Mie's series. We observe an excellent agreement between the numerical results

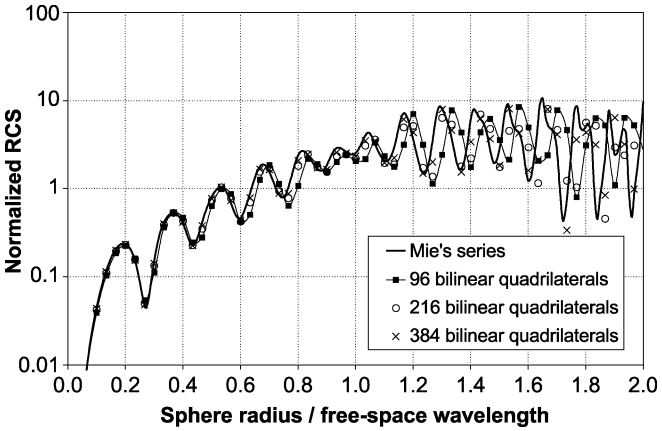

Fig. 9. Normalized radar cross-section $[\mathrm{RCS}/(a^2\pi)]$ of a dielectric $(\varepsilon_\mathrm{r} = 2.25)$ sphere, for three higher order MoM models employing the first-order geometrical modeling in Fig. 4(a)–(c), respectively, along with the exact solution (Mie's series).

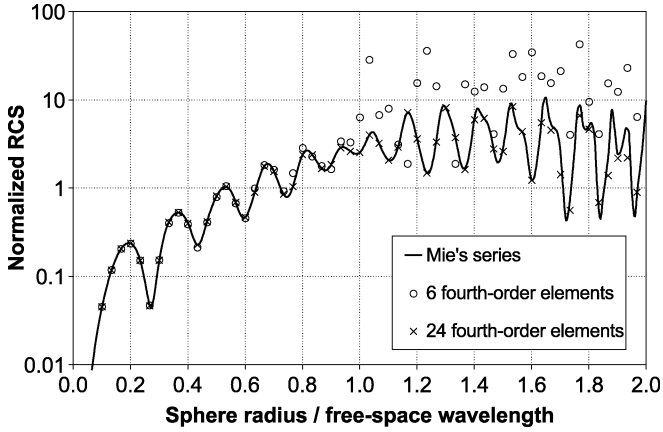

Fig. 10. Normalized radar cross-section $[\mathrm{RCS}/(a^2\pi)]$ of a dielectric $(\varepsilon_\mathrm{r} = 2.25)$ sphere, for two higher order MoM models employing the fourth-order geometrical modeling in Fig. 7(a) and (b), respectively, along with the exact solution (Mie's series).

obtained with the model (A) and analytical results up to the frequency at which $a/\lambda = 1.3$ and the curved quadrilateral elements in the model are approximately 2λ across. In particular, the maximum absolute RCS prediction error is less than 1% for $a/\lambda \leq 1.1$ (quadrilaterals are maximally 1.73λ across), and then increases slightly for $1.1 < a/\lambda \leq 1.3$. With the model (B), an excellent agreement with the exact solution is obtained in the entire frequency range considered, with the maximum absolute RCS prediction error less than 0.5% for $a/\lambda < 1.6$ and less than 3% for $a/\lambda < 2$.

Note that all the results for scattering from metallic spheres presented in this subsection are obtained by solving the EFIE (3) and no treatment of internal resonances is applied. The new double higher order method appears to yield equally accurate results at the internal resonances of the sphere, even though the condition number of the MoM matrix is very large at these frequencies. The RCS solution is sensitive to internal resonances only when the current approximation orders are not sufficient, which is also in agreement with the previous results [32].

C. Dielectric Spherical Scatterer

As an example of curved dielectric structures, consider a spherical dielectric scatterer 1 m in radius in the frequency range 10–600 MHz. The relative permittivity of the dielectric is $\varepsilon_\mathrm{r} = 2.25$ (polyethylene). Shown in Fig. 9 is the RCS of the sphere calculated using the first-order geometrical modeling $(K_u = K_v = 1)$, with the sphere surface being approximated by means of (1) $N_\mathrm{el} = 96$ bilinear quadrilaterals [Fig. 4(a)], (2) $N_\mathrm{el} = 216$ bilinear quadrilaterals [Fig. 4(b)], and (3) $N_\mathrm{el} = 384$ bilinear quadrilaterals [Fig. 4(c)], along with the analytical solution in the form of Mie's series. The adopted electric and magnetic current approximation orders in models (1), (2), and (3) are $N_u = N_v = 4$, 2, and 2 and the resulting total numbers of unknowns $N_\mathrm{unkn} = 6144$, 3456, and 6144, respectively. We observe that the RCS predictions are slightly shifted toward higher frequencies with all the three models, the frequency shift being the most pronounced with the model (1) at higher frequencies. The fact that the geometrical models are inscribed into the sphere certainly contributes to this shift of the results. Note, however, that a very good agreement can be observed between the numerical results obtained by the model (3) and the analytical results in the entire frequency range considered. Note also that the numerical results in Fig. 9 obtained by any of the three models in Fig. 4(a)–(c) are significantly more accurate than the corresponding numerical results obtained with the same models for the metallic sphere (Fig. 5), which can be attributed to the fact that inaccuracies in modeling of surfaces of penetrable (dielectric) bodies do not degrade the overall analysis results as significantly as in the case of nonpenetrable (metallic) bodies.

Fig. 10 shows the RCS of the dielectric sphere evaluated using the two fourth-order $(K_u = K_v = 4)$ geometrical models shown in Fig. 7. In the model (A), the adopted electric and magnetic current approximation orders are $N_u = N_v = 8$ $(N_\mathrm{unkn} = 1536)$, while in the model (B), these orders are set to be $N_u = N_v = 5$ $(N_\mathrm{unkn} = 2400)$. We observe that, as compared to the exact solution (Mie's series), the model (A) performs well up to the frequency at which $a/\lambda_{\mathrm{free-space}} = 0.9$ and the curved quadrilateral elements in the model are about $1.4\lambda_{\mathrm{free-space}}$ or $2.1\lambda_\mathrm{diel}$ across $(\lambda_\mathrm{diel} = \lambda_{\mathrm{free-space}}/\sqrt{\varepsilon_\mathrm{r}})$. Furthermore, the maximum absolute RCS prediction error is less than 2% for $a/\lambda_{\mathrm{free-space}} \leq 0.6$, with the maximum length of curved quadrilateral elements not exceeding $0.94\lambda_{\mathrm{free-space}}$ $(1.4\lambda_\mathrm{diel})$. The model (B) provides an accurate RCS prediction in the entire frequency range considered (quadrilaterals are $2.35\lambda_\mathrm{diel}$ across at the highest frequency), with the maximum absolute error less than 1% for $a/\lambda_{\mathrm{free-space}} < 1.26$ (maximum side dimension of quadrilaterals is about $1.5\lambda_\mathrm{diel}$) and a slightly increased error in the rest of the frequency range considered due to a minimal frequency shift of the results.

D. Wire Monopoles Attached to a Metallic Cylinder

As an example of antennas with curved surfaces, consider a system of wire monopoles attached to a metallic cylinder. The radius of the cylinder is 10 cm and its height 22 cm. The system is analyzed in two configurations: (1) with a single 12-cm monopole antenna attached to the cylinder and (2) with an 8-cm driven monopole and 44-cm parasitic monopole attached to the

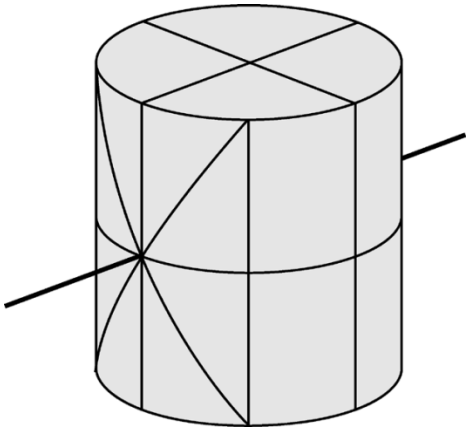

Fig. 11. Circular cylinder of finite length with attached wire monopoles, modeled by 32 biquadratic $(K_u = K_v = 2)$ quadrilaterals and two wires.

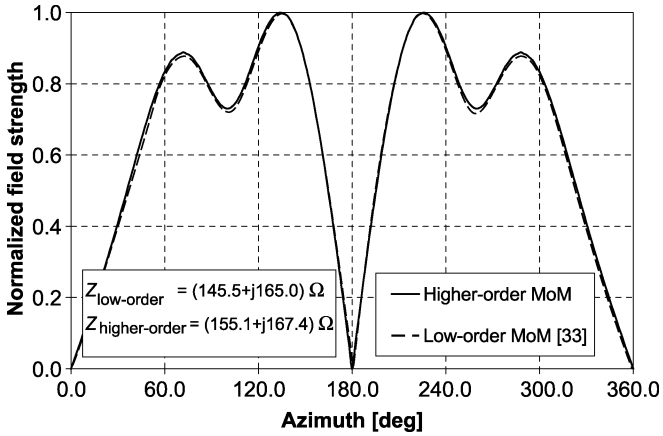

Fig. 12. Normalized far field pattern and the antenna input impedance of the antenna system in Fig. 11 with only one monopole antenna present [configuration (1)], obtained by the higher order MoM and by the low-order MoM from [33].

cylinder, as indicated in Fig. 11. The radii of the driven and passive monopoles are 1 and 2 mm, respectively. The antenna system is analyzed at the frequency of 833 MHz.

Shown in Fig. 11 is the simulated geometrical model of the structure. The cylinder is modeled using 28 and 32 second-order $(K_u = K_v = 2)$ quadrilateral surface elements in configurations (1) and (2), respectively. Each monopole is modeled by a single straight wire segment. The driven monopole is fed by a point delta generator at its base. Note that the triangle-like curved quadrilaterals are used around the wire-to-surface connections in order to easily enable current continuity across junctions. Note also that the flexibility of the generalized quadrilaterals at approximating both the curvature of the surface and the curvature of the edges of the cylinder, along with their flexibility to accommodate for degenerate quadrilateral shapes, enable the effective modeling of the cylinder with two junctions by means of only 32 surface elements. Note finally that neither the fact that the two adjacent outer edges of the quadrilaterals approximating the bases of the cylinder form an angle of 180° at the quadrilateral vertex they share nor the fact that the quadrilateral edges in the wire-to-surface junctions are extremely short (on the order of the wire radius) as compared to the other three edges of the quadrilateral do not deteriorate the accuracy of the current modeling and the overall accuracy of the analysis.

The results for the radiated far field obtained by the higher order MoM are compared with the results obtained by the low-order MoM from [33]. The patterns are shown in Fig. 12 for the configuration (1) and Fig. 13 for the configuration (2). The two-fold symmetry is used in both MoM approaches and a very good agreement of the two sets of results is observed. The discrepancy between the results is less than 3.5% in the entire pattern range in Fig. 13 and is practically nonexistent in Fig. 12. The simulation results for the monopole antenna impedance for the two configurations are given in Figs. 12 and 13 as well. We observe that the impedances computed by the two methods also agree very well. Note that the numbers of unknowns required by the higher order MoM, 49 for the configuration (1) and 62 for the configuration (2), are considerably smaller than the corresponding numbers of unknowns required by the low-order MoM [33], 936 and 986.

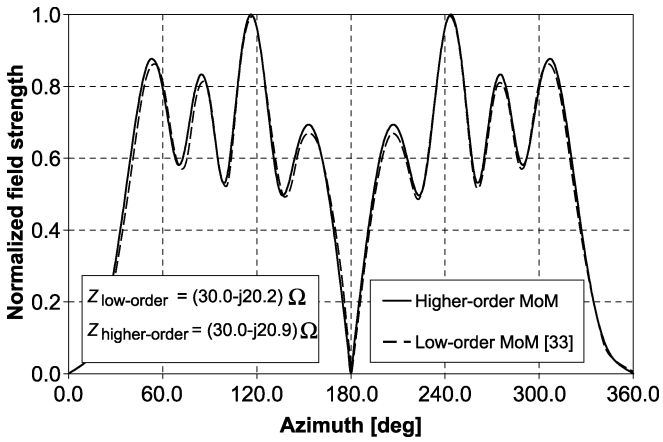

Fig. 13. Normalized far field pattern and the antenna input impedance of the antenna system in Fig. 11 with both a driven monopole and a parasitic monopole present [configuration (2)], obtained by the higher order MoM and by the low-order MoM from [33].

IV. Conclusion

This paper has proposed a highly efficient and accurate double higher order PC-oriented Galerkin-type MoM for modeling of arbitrary metallic and dielectric antennas and scatterers. The method is based on higher order geometrical modeling and higher order current modeling in the context of the SIE formulation for combined metallic (perfectly conducting) and dielectric (penetrable) structures. It employs generalized curvilinear quadrilaterals of arbitrary geometrical orders for the approximation of geometry (metallic and dielectric surfaces) and hierarchical divergence-conforming polynomial vector basis functions of arbitrary orders for the approximation of electric and magnetic surface currents within the elements. The geometrical orders and current-approximation orders of the elements are entirely independent from each other, and can be combined independently for the best overall performance of the method in different applications. The paper has presented the mathematical and computational development of the new MoM-SIE technique, including the evaluation of generalized

Galerkin impedances (MoM matrix elements) for double higher order quadrilateral boundary elements.

The accuracy, convergence, and efficiency of the new MoM-SIE technique have been demonstrated in several characteristic examples. The results obtained by the higher order MoM have been validated against the analytical solutions and the numerical results obtained by low-order MoM techniques from literature. The flexibility of the new technique has allowed for a very effective modeling of a dihedral corner reflector, a metallic spherical scatterer, a dielectric spherical scatterer, and a circular cylinder of finite length with attached wire monopoles by means of only a few large flat and curved quadrilateral boundary elements and a minimal number of unknowns. All the examples have shown excellent flexibility and efficiency of the new technique at modeling of both current variation and curvature. The examples have demonstrated advantages of large-domain models using curved quadrilaterals of high geometrical orders with basis functions of high current-approximation orders over commonly used small-domain models and existing low-order techniques from literature (the reduction in the number of unknowns is by an order of magnitude when compared to low-order solutions), but also over almost small-domain models that represent lower order versions of the proposed large-domain, high-order (more precisely, low-to-high order) technique. Finally, it has been demonstrated that both components of the double higher order modeling, i.e., higher order geometrical modeling and higher order current modeling, are essential for accurate and efficient MoM-SIE analysis of general antenna (scattering) structures.

REFERENCES

[1] R. F. Harrington, "Field computation by moment methods," in *IEEE PRESS Series on Electromagnetic Waves* Piscataway, NJ, 1993.

[2] S. M. Rao, C. C. Cha, R. L. Cravey, and D. L. Wilkes, "Electromagnetic scattering from arbitrary shaped conducting bodies coated with lossy materials of arbitrary thickness," *IEEE Trans. Antennas Propagat.*, vol. 39, pp. 627–631, May 1991.

[3] M. Analoui, M. Kagawa, and Y. Kagawa, "Electromagnetic scattering from conductor-coated material bodies," *Int. J. Numerical Modeling: Electronic Networks, Devices and Fields*, vol. 4, no. 4, pp. 287–299, Dec. 1991.

[4] S. M. Rao, T. K. Sarkar, P. Midya, and A. R. Djordjevic, "Electromagnetic radiation and scattering from finite conducting and dielectric structures: surface/surface formulation," *IEEE Trans. Antennas Propagat.*, vol. 39, pp. 1034–1037, July 1991.

[5] J. M. Song and W. C. Chew, "Moment method solutions using parametric geometry," *J. Electromagn. Waves and Applicat.*, vol. 9, no. 1/2, pp. 71–83, Jan.–Feb. 1995.

[6] R. D. Graglia, D. R. Wilton, and A. F. Peterson, "Higher order interpolatory vector bases for computational electromagnetics," *IEEE Trans. Antennas Propagat.*, vol. 45, pp. 329–342, Mar. 1997.

[7] G. Kang, J. Song, W. C. Chew, K. C. Donepudi, and J. M. Jin, "A novel grid-robust higher order vector basis function for the method of moments," *IEEE Trans. Antennas Propagat.*, vol. 49, pp. 908–915, June 2001.

[8] S. Y. Chen, W. C. Chew, J. M. Song, and J. S. Zhao, "Analysis of low frequency scattering from penetrable scatterers," *IEEE Trans. Geoscience Remote Sensing*, vol. 39, pp. 726–735, Apr. 2001.

[9] B. M. Notaroš, B. D. Popović, J. Peeters Weem, R. A. Brown, and Z. Popović, "Efficient large-domain MoM solutions to electrically large practical EM problems," *IEEE Trans. Microwave Theory Tech.*, vol. 49, pp. 151–159, Jan. 2001.

[10] B. M. Notaroš and B. D. Popović, "General entire-domain method for analysis of dielectric scatterers," in *Proc. Inst. Elect. Eng.—Microwaves, Antennas and Propagation*, vol. 143, Dec. 1996, pp. 498–504.

[11] ——, "General entire-domain Galerkin method for analysis of wire antennas in the presence of dielectric bodies," in *Proc. Inst. Elect. Eng.—Microwaves, Antennas and Propagation*, vol. 145, Feb. 1998, pp. 13–18.

[12] ——, "Large-domain integral-equation method for analysis of general 3D electromagnetic structures," *Proc. Inst. Elect. Eng.—Microwaves, Antennas and Propagation*, vol. 145, no. 6, pp. 491–495, Dec. 1998.

[13] P. De Doncker, "A potential integral equations method for electromagnetic scattering by penetrable bodies," *IEEE Trans. Antennas Propagat.*, vol. 49, pp. 1037–1042, July 2001.

[14] K. Sertel and J. L. Volakis, "Method of moments solution of volume integral equations using parametric geometry modeling," *Radio Sci.*, vol. 37, no. 1, pp. 10–17, Jan.–Feb. 2002.

[15] R. D. Graglia, "The use of parametric elements in the moment method solution of static and dynamic volume integral equations," *IEEE Trans. Antennas Propagat.*, vol. AP-36, pp. 636–646, May 1988.

[16] J. S. Savage and A. F. Peterson, "Higher-order vector finite elements for tetrahedral cells," *IEEE Trans. Microwave Theory Tech.*, vol. 44, pp. 874–879, June 1996.

[17] L. S. Andersen and J. L. Volakis, "Development and application of a novel class of hierarchical tangential vector finite elements for electromagnetics," *IEEE Trans. Antennas Propagat.*, vol. 47, pp. 112–120, Jan. 1999.

[18] J. P. Webb, "Hierarchical vector basis functions of arbitrary order for triangular and tetrahedral finite elements," *IEEE Trans. Antennas Propagat.*, vol. 47, pp. 1244–1253, Aug. 1999.

[19] J. Liu and J.-M. Jin, "A novel hybridization of higher order finite element and boundary integral methods for electromagnetic scattering and radiation problems," *IEEE Trans. Antennas Propagat.*, vol. 49, pp. 1794–1806, Dec. 2001.

[20] M. M. Ilić and B. M. Notaroš, "Higher order hierarchical curved hexahedral vector finite elements for electromagnetic modeling," *IEEE Trans. Microwave Theory Techniques*, vol. 51, pp. 1026–1033, Mar. 2003.

[21] M. Djordjević and B. M. Notaroš, "Higher-order moment-method modeling of curved metallic antennas and scatterers," in *Proc. IEEE Antennas and Propagation Society Int. Symp. Dig.*, vol. 4, Columbus, OH, June 22–27, 2003, pp. 94–97.

[22] P. P. Silvester and R. L. Ferrari, *Finite Elements for Electrical Engineers*. Cambridge, U.K.: Cambridge Univ. Press, 1996.

[23] M. Salazar-Palma, T. P. Srkar, L. E. Garcia-Castillo, T. Roy, and A. Djordjević, *Iterative and Self-Adaptive Finite Elements in Electromagnetic Modeling*. Boston, MA: Artech House, 1998.

[24] R. D. Graglia, P. L. E. Uslenghi, R. Vitiello, and U. D'Elia, "Electromagnetic scattering for oblique incidence on impedance bodies of revolution," *IEEE Trans. Antennas Propagat.*, vol. 43, pp. 11–26, Jan. 1995.

[25] J. C. Nedelec, "Mixed finite elements in R3," *Numerische Mathematik*, vol. 35, pp. 315–341, 1980.

[26] M. Djordjević and B. M. Notaroš, "Three types of higher-order MoM basis functions automatically satisfying current continuity conditions," in *Proc. IEEE Antennas and Propagation Society Int. Symp. Digest*, San Antonio, TX, June 16–21, 2002, pp. 610–613.

[27] ——, "Higher-order hierarchical basis functions with improved orthogonality properties for moment-method modeling of metallic and dielectric microwave structures," *Microwave Opt. Technol. Lett.*, vol. 37, no. 2, pp. 83–88, Apr. 2003.

[28] B. M. Notaroš and B. D. Popović, "Optimized entire-domain moment-method analysis of 3D dielectric scatterers," *Int. J. Numerical Modelling: Electronic Networks, Devices and Fields*, vol. 10, pp. 177–192, May–June 1997.

[29] ——, "Generalized excitations and loads for electromagnetic analysis with boundary elements," *Int. J. Engineering Analysis With Boundary Elements, ELSEVIER: Special Issue on Electromagnetics*, vol. 27, no. 4, pp. 333–343, Apr. 2003.

[30] T. Griesser, C. A. Balanis, and L. Kefeng, "RCS analysis and reduction for lossy dihedral corner reflectors," *Proc. IEEE*, vol. 77, no. 5, pp. 806–814, May 1989.

[31] S. M. Rao, D. R. Wilton, and A. W. Glisson, "Electromagnetic scattering by surfaces of arbitrary shape," *IEEE Trans. Antennas Propagat.*, vol. AP-30, pp. 409–418, May 1982.

[32] F. X. Canning, "Protecting EFIE-based scattering computations from effects of interior resonances," *IEEE Trans. Antennas Propagat.*, vol. 39, pp. 1545–1552, Nov. 1991.

[33] R. E. Hodges and Y. Rahmat-Samii, "An iterative current-based hybrid method for complex structures," *IEEE Trans. Antennas Propagat.*, vol. 45, pp. 265–276, Feb. 1997.

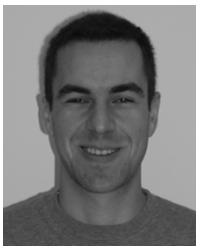

Miroslav Djordjević (S'00–M'04) was born in Ćuprija, Serbia and Montenegro (former Yugoslavia), in 1973. He received the Dipl.Ing. (B.S.) degree from the University of Belgrade, Belgrade, Serbia and Montenegro, in 1998, the M.S. degree from the University of California, Los Angeles (UCLA), in 2000, and the Ph.D. degree from the University of Massachusetts (UMass) Dartmouth, in 2004.

From 1998 to 2000, he was a Graduate Student Researcher at the Antenna Research and Measurement (ARAM) Laboratory, UCLA. Since 2000 to 2003, he was a Research Assistant at UMass where he is currently a Postdoctoral Associate. His research interests are in higher order modeling, hybrid methods, and analysis of vehicle mounted antennas.

Branislav M. Notaroš (M'00–SM'03) was born in Zrenjanin, Yugoslavia, in 1965. He received the Dipl.Ing. (B.Sc.), M.Sc., and Ph.D. degrees in electrical engineering from the University of Belgrade, Belgrade, Yugoslavia, in 1988, 1992, and 1995, respectively.

He is currently an Assistant Professor of electrical and computer engineering with the University of Massachusetts Dartmouth. From 1996 to 1998, he was an Assistant Professor with the Department of Electrical Engineering, University of Belgrade. He spent the 1998 to 1999 academic year as a Visiting Research Associate with the University of Colorado at Boulder. His teaching activities are in the area of theoretical and applied electromagnetics. He is the Co-Director of the Telecommunications Laboratory, Advanced Technology and Manufacturing Center, University of Massachusetts Dartmouth. He has authored or coauthored 15 journal papers, 40 conference papers, a book chapter, five university textbooks and workbooks, and a conceptual assessment tool for electromagnetics education. His research interests are predominantly in computational electromagnetics and antenna design.

Dr. Notaroš was the recipient of the 1999 Institution of Electrical Engineers (IEE) Marconi Premium.